Venus: A Thick Basal Magma Ocean May Exist Today

J. G. O'Rourke[1]

[1]School of Earth and Space Exploration, Arizona State University, Tempe, AZ, USA.

Corresponding author: J. G. O'Rourke (jgorourk@asu.edu)

Key Points:

- Extensive melting of the deep mantle during Earth's accretion and differentiation was proposed to solve geochemical and geodynamic puzzles
- High temperatures and slow mantle cooling relative to Earth naturally extend the predicted lifetime of a basal magma ocean in Venus
- A basal magma ocean in Venus would sequester incompatible elements such as potassium and argon and may have sustained a dynamo

Abstract

Basal magma oceans develop in Earth and Venus after accretion as their mantles solidify from the middle outwards. Fractional crystallization of the basal mantle is buffered by the core and radiogenic and latent heat in the magma ocean. Previous studies showed that Earth's basal magma ocean would have solidified after two or three billion years. Venus has a relatively hot interior that cools slowly in the absence of plate tectonics, which reduces heat flow through the solid mantle. Consequentially, the basal magma ocean could remain as thick as ~200–400 km today. Vigorous convection of liquid silicates could power a global magnetic field until recently while a core-hosted dynamo is suppressed. The basal magma ocean may be a hidden reservoir of potassium and other incompatible elements. A high tidal Love number could reveal a basal magma ocean and would definitively establish that the core is at least partially liquid.

Plain Language Summary

Venus is Earth's nearest neighbor but arguably the least-studied planet in the inner solar system. Although there are no direct constraints on its deep structure, the mantle of Venus is assumedly solid by analogy to Earth's current condition. However, recent models of Earth focus on the prospect that a thick layer of melt called a "basal magma ocean" persisted in the lowermost mantle for billions of years. This layer cools orders-of-magnitude more slowly than a magma ocean near the surface because the solid mantle acts as a ~3000-km-thick blanket. Moreover, the solid mantle itself remains hot in Venus compared to Earth because its surface is scorched and desiccated. This study argues that the lifetime of the basal magma ocean in Venus plausibly extends to the present. Detecting a thick, molten layer with future spacecraft missions would support the hypothesis that Venus and Earth formed under similarly energetic conditions.

1 Introduction

Magma oceans were ubiquitous during the formation of rocky planets. Giant impacts, radiogenic heating, and core formation melted entire mantles (e.g., Canup, 2012; Ćuk & Stewart, 2012; Elkins-Tanton, 2012; Nakajima & Stevenson, 2015). Crystallization of the mantle proceeded from the middle outwards because melt is gravitationally stable near both the surface and core/mantle boundary (CMB) (e.g., Labrosse et al., 2007; Stixrude & Karki, 2005). Bridgmanite crystals are neutrally buoyant at mid-mantle depths (e.g., Caracas et al., 2019; Mosenfelder et al., 2007). Surficial magma oceans solidify within ~100 Myr via rapid cooling to space (e.g., Hamano et al., 2013). However, a basal magma ocean (BMO) can survive for billions of years because cooling through the solid mantle is orders-of-magnitude less efficient.

Earth's putative BMO has received scrutiny because liquid silicates are a reservoir of incompatible elements. Labrosse et al. (2007) proposed that a long-lived BMO could explain differences in $^{142}Nd/^{144}Nd$ ratios between terrestrial rocks and chondritic meteorites and solve the so-called "missing heat source" problem (e.g., Korenaga, 2008). Primordial iron-rich melt (e.g., Zhang et al., 2016) and compositional anomalies (e.g., Li et al., 2017) in the deep mantle are possibly the last residua of a BMO that has almost finished solidifying.

Models that feature a terrestrial BMO predict suppressed cooling of the core and a delayed start for the geodynamo. Because the BMO has low viscosity, the thermal contrast across the CMB is negligible (e.g., Ulvrová et al., 2012). That is, the BMO and uppermost core should have the same temperature and must cool in tandem. Latent and radiogenic heat in the BMO buffers its cooling rate, so the core cannot cool rapidly enough to drive thermal convection

until the BMO has started solidifying. Assuming the BMO was well-mixed, Labrosse et al. (2007) suggested that Earth's core would not convect until ~3.4–4 Gyr ago. Compositional stratification in the BMO could lead to non-continuous dynamo operation with a brief burst of activity before an extended pause (Laneuville et al., 2017). For now, whether a dynamo existed in the Hadean and/or Eoarchean is unknown (e.g., Tang et al., 2019; Weiss et al., 2015).

Why would Earth but not Venus have a BMO? These two planets have nearly identical sizes and bulk densities that plausibly reflect similar bulk compositions (e.g., Smrekar et al., 2018). Venus likely suffered energetic impacts during accretion although they produced no moon (e.g., Gillmann et al., 2016; Jacobson et al., 2017). Regardless, gravitational and radiogenic heating alone were sufficient to melt the primordial mantle (e.g., Elkins-Tanton, 2012; Ikoma et al., 2018). Habitable conditions may have continued until ~1 Gyr ago on Venus (e.g., Way et al., 2016). Alternatively, the proximity of Venus to the Sun may have delayed solidification of the surficial magma ocean (e.g., Hamano et al., 2013) and desiccated the atmosphere and surface (e.g., Gillmann et al., 2009). In the absence of colder temperatures and oceans, Venus entered a geodynamic regime that is less efficient at cooling the mantle than plate tectonics. Models indicate that the heat flow from the solid mantle to the surface in Venus is roughly half Earth's modern value, i.e., ~20 TW versus 44 TW (e.g., Driscoll & Bercovici, 2013, 2014; Gillmann & Tackley, 2014; Weller & Kiefer, 2019). A BMO should have formed inside Venus and would solidify at a slower rate over time.

Ultimately, the prospect that a major feature such as a BMO could await detection highlights the pressing need to explore Earth's near twin.

2 Methods

Figure 1 illustrates the imagined internal structure of Venus. Broadly speaking, the compositional layering of the deep interior resembles that of Earth roughly two billion years ago. No inner core has yet nucleated within Venus—Earth's core only began freezing from the inside out within the past billion years (e.g., Labrosse, 2015; Nimmo, 2015; O'Rourke et al., 2017). Fractional crystallization of the BMO enriched the lower mantle in iron. Convection in the solid mantle of Venus may have organized iron-rich material into thermochemical piles (e.g., Labrosse et al., 2007; Li et al., 2017), while the BMO itself remains thick enough to constitute a global layer with limited topography. However, structural similarities give way to dynamical differences because modern Venus cools slowly compared to middle-aged Earth. Crucially, the core and BMO of Venus are entirely stagnant or convecting too sluggishly to drive a dynamo.

2.1. Thermal histories

Parameterizations of energy sources and sinks track the thermochemical evolution of the BMO and core. The Supporting Information describes how Labrosse et al. (2007) and O'Rourke et al. (2018) were adapted. Briefly, the heat budget of the BMO is

$$Q_{BMO} = Q_{SM} + Q_{RM} + Q_{LM} + Q_{CMB}, \quad (1)$$

where the heat flow across the solid/liquid interface in the basal mantle (Q_{BMO}) is a boundary condition. Instead of using parameterizations of mantle convection (e.g., in the stagnant- or episodic-lid regimes for Venus), Q_{BMO} is assumed to decrease linearly over time. For this study, this simplification is adequate because the present-day thickness of a BMO mostly depends on the total amount of cooling rather than on details of the thermal history, which are highly

uncertain for Venus. The first three terms on the right side represent secular cooling (Q_{SM}), radiogenic heating (Q_{RM}), and latent heat (Q_{LM}) in the BMO (e.g., Labrosse et al., 2007; Ziegler & Stegman, 2013). The heat flow across the CMB (Q_{CMB}) comprises additional terms that describe the energy budget of the core (e.g., Labrosse, 2015; O'Rourke et al., 2018):

$$Q_{CMB} = Q_{SC} + Q_{RC} + Q_{PC} + Q_{GC} + Q_{LC} + Q_{IC}, \quad (2)$$

which include secular cooling of the outer core (Q_{SC}), radiogenic heating (Q_{RC}), and precipitation of light species such as magnesium oxide near the CMB (Q_{PC}). After nucleation, the inner core contributes gravitational energy from the exclusion of light elements (Q_{GC}), latent heat (Q_{LC}), and secular cooling under the assumption of efficient thermal conduction (Q_{IC}). Terms representing the heat of reaction and pressure changes from thermal contraction are considered negligible (e.g., Blanc et al., 2019). Exothermic reactions between the core and BMO such as oxygen partitioning (e.g., Pozzo et al., 2019) are also ignored, but could also slow the solidification of the BMO. Large amounts of heat could be transported laterally within the BMO and core and/or conducted upwards. However, the energy budgets only include heat that crosses the CMB or the upper boundary of the BMO because heats that are generated and lost within a single layer sum to zero. Labrosse et al. (2007) assumed that Q_{CMB} was proportional to one specific heat for the core, which was held constant. In reality, the effective specific heat of the core should decrease over time with radiogenic heating but increase once the inner core nucleates. This study avoids that simplification in order to delineate the inner core and dynamo.

The key to generating thermal histories is realizing that nearly all of the heat sources are directly proportional to the cooling rate of the core. Radiogenic heating is the exception but easy to calculate from the abundances of heat-producing elements. For all other terms in Eq. 1,

$$Q_i = \tilde{Q}_i \left(\frac{dT_C}{dt} \right), \quad (3)$$

where $\tilde{Q}_i$ depends only on the thermodynamic properties of the BMO and core (i.e., physical constants from Tables S1 and S2) and T_C is the temperature at the CMB. Secular cooling in the BMO is parameterized using a specific heat that is invariant with depth. Latent heat is computed with an idealized phase diagram for a well-mixed BMO (Labrosse et al., 2007). Energetic terms for the core are derived by integrating fourth-order polynomials, which describe the radial density and temperature profiles in the core, over the volume(s) of the outer and/or inner cores (e.g., Labrosse, 2015; Nimmo, 2015; O'Rourke et al., 2018). Combining Eq. 1 and 2,

$$\frac{dT_C}{dt} = \frac{Q_{BMO} - Q_{RM} - Q_{RC}}{\tilde{Q}_{SM} + \tilde{Q}_{LM} + \tilde{Q}_{SC} + \tilde{Q}_{PC} + \tilde{Q}_{GC} + \tilde{Q}_{LC} + \tilde{Q}_{IC}} . \quad (4)$$

This equation places the boundary and initial conditions in the numerator and the structural parameters in the denominator. As discussed in the Supporting Information, the thickness of the BMO and the radius of the inner core are also directly proportional to dT_C/dt. Given initial values for the size of the BMO and T_C, the forward Euler method generates a thermal history consisting of all the time-dependent quantities listed in Table S3. Timesteps of ~0.5 Myr suffice because halving the timestep yielded no discernable change in the model results.

Technically, Equations 2–4 are valid only if the core is well-mixed and isentropic. Stable stratification in the core develops once Q_{CMB} becomes sub-adiabatic (e.g., Labrosse, 2015; Nakagawa, 2018) and/or the uppermost core is enriched in light elements (e.g., Buffett & Seagle, 2010; Gubbins & Davies, 2013; Helffrich, 2014; O'Rourke & Shim, 2019). Nakagawa (2018)

showed that diffusion and double-diffusive processes in a stratified region trap heat that is conducted upwards from lower regions in the core, acting as an extra heat sink. Models that include stratification predict relatively high T_C over time, slow growth of an inner core, and less magnetic dissipation in the core. Here, stratification is not explicitly modeled, which provides conservative estimates for the lifespan of the BMO and the likelihood of a dynamo in the core.

2.2. Prospects for dynamo action

Thermal histories reveal when and where a dynamo could exist. The basic criterion for a dynamo is a rapidly rotating, electrically conductive fluid convecting with sufficient vigor. Although the rotation of Venus is "slow" relative to Earth, it is "rapid" in the context of dynamo physics because the Coriolis force would strongly affect flow in its core and/or BMO given small Rossby numbers ($\sim 10^{-5} << 1$) at the equator (e.g., Stevenson, 2003). Simply put, the rotation rate of Venus is not to blame for the lack of a dynamo. If the heat flow across the upper boundary does not exceed that conducted upwards along an adiabatic gradient, then thermal conduction—the bane of dynamos—transports heat without fluid motion. Chemical sources of buoyancy such as radiogenic heating, precipitation of light elements, and growth of an inner core decrease the minimum heat flow required to support a dynamo relative to the adiabatic limit.

There are two general methods for estimating the power of a dynamo. First, scaling laws relate the flux of compositional and/or thermal buoyancy to the velocities of convective flows (e.g., Christensen, 2010). Higher velocities translate to stronger magnetic fields. Second, entropy budgets reveal whether non-zero amounts of dissipation are available for the dynamo (e.g., Labrosse, 2015). Classical thermodynamics explicitly compares the entropy sink associated with thermal conductivity to the entropy production from the myriad heat sources. To enable straightforward comparisons to previous studies, velocity scalings are applied to the BMO (e.g., Labrosse et al., 2007; Ziegler & Stegman, 2013) while the entropy budget is calculated for the core (e.g., O'Rourke et al., 2018). In contrast, Driscoll & Bercovici (2014) used velocity scalings for the core while Blanc et al. (2019) recently formulated the entropy budget for the BMO. Either method yields similar results. Ultimately, no dynamo exists when the heat flow is sub-critical.

Velocity scalings quantify convective vigor within the BMO. The magnetic Reynolds number is $\mathrm{Rm} = \mu_0 v_M h_M \sigma_M$. A dynamo may exist if $\mathrm{Rm} > O(10)$, where an exact cutoff of 40 is popular (e.g., Stevenson, 2003). Here μ_0 is the permittivity of free space and h_M is the thickness of the BMO (e.g., Ziegler & Stegman, 2013). The electrical conductivity (σ_M) is assumed to equal 2×10^4 S/m (Holmström et al., 2018; Scipioni et al., 2017; Soubiran & Militzer, 2018). The scaling based on the Coriolis-Inertial-Archimedean (CIA) force balance provides preferred values for the convective velocity (v_M):

$$v_{CIA} = \left(\frac{Q_{BMO}}{\rho_M H_T}\right)^{\frac{2}{5}} \left(\frac{h_M}{\Omega}\right)^{\frac{1}{5}}, \tag{5}$$

where ρ_M is the density of the BMO, H_T is its thermal scale height, and Ω is the planetary rotation rate. Scalings based on mixing length theory and the Magnetic-Archimedean-Coriolis (MAC) force balance are also considered (Supporting Information). If the Rm-criterion is satisfied, then the magnetic field at the equatorial surface is calculated as

$$B_S = \frac{1}{7}(2\epsilon f_{ohm} \mu_0 \rho_M v_{CIA}^2)^{\frac{1}{2}} \left(\frac{r_B}{r_P}\right)^3, \tag{6}$$

where ε is a constant prefactor, f_{ohm} is the fraction of available power that is converted to ohmic dissipation as magnetic energy, r_B is the radial distance from the planetary center to the upper boundary of the BMO, and r_P is the planetary radius (Christensen, 2010). These scalings predict Earth-like surface strengths of ~30 μT for flow velocities of ~1 cm/s in the BMO.

Entropy budgets determine whether the core is convective. The total dissipation available for a dynamo is the sum of various sources and sinks:

$$\Phi = \frac{T_{DC}[T_L(r_I) - T_C]}{T_L(r_I)T_C}(Q_{LC} + Q_{IC}) + \frac{T_{DC}}{T_C}(Q_{GC}) + \frac{T_{DC} - T_C}{T_C}(Q_{RC}) + \frac{T_{DC}(T_{SC} - T_C)}{T_{SC}T_C}(Q_{SC}) + \frac{T_{DC}}{T_C}(Q_{PC}) - T_{DC}E_K. \quad (7)$$

Here T_{DC} is the average temperature in the outer core, $T_L(r_I)$ is the liquidus temperature of the core at the inner core boundary, and T_{SC} is an effective temperature association with dissipation from secular cooling. The entropy sink (E_K) is associated with and directly proportional to thermal conductivity. The thermal conductivity of the core near the CMB is uncertain within a broad range: ~33–226 W/m/K (e.g., Konôpková et al., 2016; Ohta et al., 2016). In contrast, the thermal conductivity of perovskite at similar conditions is unambiguously lower at ~10–20 W/m/K (e.g., Ohta et al., 2012). Gravitational energies associated with chemical buoyancy (Q_{GC} and Q_{PC}) are efficient sources of dissipation that are not penalized by "Carnot-like" efficiency terms (e.g., Labrosse, 2015; O'Rourke et al., 2018). The total dissipation is translated into a true dipole moment (TDM) using a scaling law that considers the relative amounts of dissipation generated at the CMB and inner core boundaries (Aubert et al., 2009). This scaling is only approximate because how the dynamo changes once the inner core nucleates remains uncertain (e.g., Landeau et al., 2017). The intensity of the magnetic field at the equatorial surface is

$$B_S = \frac{\mu_0}{4\pi}\left(\frac{\mathrm{TDM}}{r_P^3}\right). \quad (8)$$

Magnetohydrodynamic couplings may exist between flows in the core and BMO, but these formulations assume they are independent.

3 Results

3.1. Earth

Earth is a benchmark for models of Venus. Augmenting Labrosse et al. (2007) with a detailed description of the core was the first step in this study. The nominal model was initialized with the thickness and temperature of the BMO equaling 750 km and 5250 K, respectively. The BMO started with 20 TW of radiogenic heating, which is ~14% of the total heating expected for bulk silicate Earth (e.g., Lay et al., 2008). The core contained 50 ppm of potassium (e.g., Hirose et al., 2013) and precipitated light elements at a rate of ~10^{19} kg/K or 5 × 10^{-6} K^{-1} normalized to the mass of the core (e.g., Badro et al., 2018; O'Rourke & Stevenson, 2016). Finally, Q_{BMO} decreased linearly from 55 TW at the start to 15 TW at present, which approximates the cooling history obtained using boundary layer models (e.g., Blanc et al., 2019; Labrosse et al., 2007; Ziegler & Stegman, 2013) and dynamical simulations (e.g., Nakagawa & Tackley, 2010, 2015).

Figure S1 shows that this model reproduces major features of Earth's history. First, the globally averaged thickness of the BMO is only ~1 km at present (Figure S1c), which is small

enough that solid-state mantle convection would concentrate the BMO into pockets of primordial melt consistent with seismology (Labrosse et al., 2007). Second, the predicted radius of the inner core today is 1206 km, close to the correct value of 1220 km (Figure S1d). Third, the inner core nucleated ~500 Myr ago (Figure S1e) but a dynamo persisted at all times (Figure S1f). If the thermal conductivity of the core is relatively low at ~40 W/m/K, then a core dynamo always operated. Higher thermal conductivity could suppress a core dynamo at early times, but the BMO would still host a dynamo with roughly the same strength for the first ~0.5–1.5 Gyr (Figure S1f).

Figure S2 reports a sensitivity test for the terrestrial models. Initial values of h_M and Q_{BMO} were varied from ~600 to 1500 km and ~35 to 60 TW, respectively. Decreasing the heat flow to the solid mantle is equivalent to decreasing the amount of radiogenic heating and/or the latent heat of solidification in the BMO, so those other parameters were not separately permuted. Key outputs were the present-day thickness of the BMO (Figure S2a) and the lifetime of the dynamo in the BMO (Figure S2b). Neither key output was very sensitive to the initial temperature of the BMO. Likewise, the thermal history of the BMO does not depend on the particulars of the evolution of the core. For example, changing the amount of radiogenic heating or the rate of elemental precipitation only adjusts the proportions in which the available heat flow (Q_{CMB}) is distributed between the various sources. Models are invalidated if $h_M \geq 10$ km today because seismology has revealed no global melt layer in the basal mantle. Ultimately, Earth's BMO could have started as thick as ~1000 km, in which case a dynamo in the BMO may have survived for ~2 Gyr. Assuming that Earth and Venus accreted in an equivalently energetic environment, expecting that the BMO in Venus began with a similar size seems logical.

3.2. Venus

A nominal model for Venus was obtained through two modifications to the terrestrial benchmark. First, various structural parameters were adjusted to slightly lower internal pressures (Table S2), i.e., ~125 versus 130 GPa at the CMB for Venus and Earth, respectively. Second, T_C = 4900 K initially and the heat flow to the solid mantle was halved at all times, i.e., Q_{BMO} decreased linearly from 27 to 7 TW over 4.5 Gyr to match the cooling history in dynamical simulations (e.g., Gillmann & Tackley, 2014; O'Rourke et al., 2018). The initial thickness of the BMO remained 750 km. These treatments are faithful to the hypothesis that Venus and Earth began as twins but diverged as their surficial magma oceans solidified on different timescales.

Figure 2 elucidates the structure and dynamics of the deep interior. Radiogenic and latent heat dominate the energy budget of the BMO (Fig. 2a), which only cools by ~233 K over 4.5 Gyr (Fig. 2b). The thickness of the BMO decreases to ~234 km (Fig. 2c)—still deep enough to constitute a global layer. Temperatures at the liquid-solid interface atop the BMO (T_M) are estimated by averaging the solidus and liquidus of peridotite (Rubie et al., 2015). Figure S3 connects this model to earlier estimates of the thermal state of the solid mantle. A thermal boundary layer must exist at the base of the solid mantle. Otherwise, the potential temperature of the mantle would imply unrealistically high rates of surface volcanism. Driving a dynamo in the core with thermal convection alone requires $Q_{CMB} > 4.5$ TW compared to its maximum and modern values of ~2.4 and 1.7 TW, respectively. Dissipation in the core is negative always (Fig. 2d) even with the thermal conductivity set to the lowest plausible value (40 W/m/K). If there were no BMO, then $Q_{CMB} \sim Q_{BMO}$ and the core would produce a dynamo. The BMO may have hosted a dynamo until recently, although the predicted lifetime is highly sensitive to the velocity scaling law (Fig. 2e). Mixing length theory suggests that a strong dynamo existed until only ~0.2 Myr ago. In contrast, the MAC scaling indicates that the dynamo died ~2.8 Gyr ago. The

(favored) CIA scaling predicts a magnetic field with surface strengths of ~10–30 μT until ~1 Gyr ago, the estimated average age of surface units (e.g., McKinnon et al., 1997).

Figure 3 shares a sensitivity test for these models of Venus. Initial values of h_M and Q_{BMO} were varied again (Fig. 3a and 3c), alongside a range of starting values for T_C (Fig. 3b and 3d). Models were invalidated if the CIA scaling predicted that the BMO would host a dynamo today because Rm > 40. The derived upper limits on the initial thickness of the BMO are similar for Earth and Venus although the criterion for Earth was nearly complete solidification of the BMO. For Venus, setting $h_M \leq 860$ km initially would yield acceptable models using the nominal cooling history, which return $h_M \leq 370$ km at present day. The upper limit for h_M increases to ~1250 km but decreases to ~630 km if Q_{BMO} is raised or lowered initially to 40 or 20 TW, respectively. As for Earth, these results are mostly insensitive to the absolute temperature of the BMO. Changing T_C by ~1500 K is equivalent to adjusting Q_{BMO} by ~3 TW only, so the a priori uncertainty on T_C is relatively unimportant albeit very large.

Cooling timescales are also highly sensitive to assumptions about the chemistry of the solidifying BMO. One parameter describes a simplified linear phase diagram: $\Delta\phi$, the change in the mass fraction of the iron-rich component upon freezing (Supporting Information). These models assume $\Delta\phi = 0.088$ (Labrosse et al. 2007). Lowering $\Delta\phi$ means that a given cooling rate corresponds to faster solidification of the BMO. For example, redoing the nominal model for Venus with $\Delta\phi = 0.05$ (Ziegler & Stegman 2013) yields $h_M = 152$ km and $T_C = 4772$ K today. The predicted lifetime of a dynamo in the BMO is shortened by ~0.5 Gyr. Future work should incorporate a detailed phase diagram with a realistic partition coefficient for FeO between the BMO and the solid mantle (e.g., Blanc et al., 2019) and track any compositional layering (e.g., Laneuville et al., 2017). Fully dynamical simulations could generate self-consistent cooling histories for the entire planet and reveal the fate of iron-rich residua in the solid mantle.

4 Discussion

The likelihood that a BMO persisted within Venus has myriad implications. In particular, incompatible elements from the lowermost ~650–1250 km of the mantle (e.g., ~11–25% of the mantle's total volume), including potassium and decay products such as argon-40 (e.g., Kaula, 1999; Namiki & Solomon, 1998; O'Rourke & Korenaga, 2015; Xie & Tackley, 2004), could remain hidden in a reservoir unsampled by surface volcanism and degassing. Beyond geochemistry, two issues deserve attention.

4.1. Tidal response

Tidal deformation of Venus constrains the structure of the deep interior. Assuming an elastic response from the mantle to solar tides, Yoder (1995) predicted that a Love number k_2 above 0.23 would signal that the core is at least partially liquid today. Doppler tracking of the NASA Magellan and Pioneer Venus Orbiter missions then determined that $k_2 = 0.295 \pm 0.066$ (Konopliv & Yoder, 1996). However, Dumoulin et al. (2017) recently showed that realistic viscoelasticity of the mantle strongly increases k_2 relative to predictions from elastic models—envisioned missions would need to constrain $k_2 > 0.27$ to verify that the core is liquid. A BMO would decouple the solid mantle from the core and, in principle, raise k_2 even if the underlying core were completely solid. In reality, the solidus of the core is initially far lower than that of the basal mantle and further decreases as the growing inner core concentrates impurities in the

remaining liquid. No realistic thermal history features a BMO and a solid core (O'Rourke et al., 2018). Measuring a high k_2 would prove that the core remains partially liquid.

4.2. Magnetic history

Venus may have sustained an Earth-strength magnetic field until recently. O'Rourke et al. (2018) found that the core would power a dynamo for billions of years absent a BMO. High thermal conductivity for the core (>100 W/m/K) was invoked because simulations using lower conductivities over-predicted the dynamo's lifetime. Here, a dynamo exists instead in the BMO but survives for similar timescales. Thermal conductivity of the core is no longer a critical uncertainty because the cooling rate of the core is sub-adiabatic regardless. Crustal remanent magnetism is a potentially observable consequence of an early dynamo in either the core or BMO (O'Rourke et al., 2019). Alternatively, Venus could have accreted under less energetic conditions where any BMO was short-lived and chemical stratification precluded convection in the core (Jacobson et al., 2017), meaning no crustal remanence would exist.

5 Conclusions

Earth's early evolution featured a basal magma ocean that took several billion years to solidify. Until now, these models have not been extended to Venus. Slow mantle cooling in the absence of plate tectonics on Venus is a common feature of dynamical simulations. The natural consequence is an extended lifetime for the basal magma ocean. Halving the cooling rate approximately doubles the solidification timescale. The lowermost ~200–400 km of the mantle plausibly remain molten today. Seismology would enable the direct detection of a thick melt layer, which should also yield a high tidal Love number that is degenerate with a partially liquid core. The basal magma ocean is a hidden reservoir of incompatible elements that the solid mantle will not ingest for billions of years. Vigorous fluid motions in the basal magma ocean can drive a dynamo until recent times (<1 Gyr ago), but latent and radiogenic heat keeps the cooling rate of the core below the adiabatic limit for a dynamo driven by thermal convection. The basal magma ocean gives, and the basal magma ocean has taken away.

Acknowledgments

J. G. O'Rourke was supported by the SESE Exploration Postdoctoral Fellowship at Arizona State University. Data sharing is not applicable to this article as no new data were created or analyzed in this study. Jupyter notebooks that run the models for Earth and Venus to generate Figures 2, 3, S1, and S2 are archived on GitHub (github.com/jgorourke/Venus-BMO). An anonymous reviewer and D. Stegman provided many helpful comments.

References

Aubert, J., Labrosse, S., & Poitou, C. (2009). Modelling the palaeo-evolution of the geodynamo. *Geophysical Journal International*, *179*(3), 1414–1428. https://doi.org/10.1111/j.1365-246X.2009.04361.x

Badro, J., Aubert, J., Hirose, K., Nomura, R., Blanchard, I., Borensztajn, S., & Siebert, J. (2018). Magnesium Partitioning Between Earth's Mantle and Core and its Potential to Drive an Early Exsolution Geodynamo. *Geophysical Research Letters*, *45*(24), 13,240-13,248. https://doi.org/10.1029/2018GL080405

Blanc, N. A., Stegman, D. R., & Ziegler, L. B. (2019). Thermal and Magnetic Evolution of a Crystallizing Basal Magma Ocean in Earth's Mantle. https://doi.org/10.31223/osf.io/cmgef

Buffett, B. A., & Seagle, C. T. (2010). Stratification of the top of the core due to chemical interactions with the mantle. *Journal of Geophysical Research*, *115*(B4), B04407. https://doi.org/10.1029/2009JB006751

Canup, R. M. (2012). Forming a Moon with an Earth-like composition via a giant impact. *Science*, *338*(6110), 1052–5. https://doi.org/10.1126/science.1226073

Caracas, R., Hirose, K., Nomura, R., & Ballmer, M. D. (2019). Melt–crystal density crossover in a deep magma ocean. *Earth and Planetary Science Letters*, *516*, 202–211. https://doi.org/10.1016/j.epsl.2019.03.031

Christensen, U. R. (2010). Dynamo Scaling Laws and Applications to the Planets. *Space Science Reviews*, *152*(1–4), 565–590. https://doi.org/10.1007/s11214-009-9553-2

Ćuk, M., & Stewart, S. T. (2012). Making the Moon from a fast-spinning Earth: a giant impact followed by resonant despinning. *Science*, *338*(6110), 1047–52. https://doi.org/10.1126/science.1225542

Driscoll, P., & Bercovici, D. (2013). Divergent evolution of Earth and Venus: Influence of degassing, tectonics, and magnetic fields. *Icarus*, *226*(2), 1447–1464. https://doi.org/10.1016/j.icarus.2013.07.025

Driscoll, P., & Bercovici, D. (2014). On the thermal and magnetic histories of Earth and Venus: Influences of melting, radioactivity, and conductivity. *Physics of the Earth and Planetary Interiors*, *236*, 36–51. https://doi.org/10.1016/j.pepi.2014.08.004

Dumoulin, C., Tobie, G., Verhoeven, O., Rosenblatt, P., & Rambaux, N. (2017). Tidal constraints on the interior of Venus. *Journal of Geophysical Research: Planets*, *122*(6), 1338–1352. https://doi.org/10.1002/2016JE005249

Elkins-Tanton, L. T. (2012). Magma Oceans in the Inner Solar System. *Annual Review of Earth and Planetary Sciences*, *40*(1), 113–139. https://doi.org/10.1146/annurev-earth-042711-105503

Gillmann, C., & Tackley, P. (2014). Atmosphere/mantle coupling and feedbacks on Venus. *Journal of Geophysical Research: Planets*, *119*(6), 1189–1217. https://doi.org/10.1002/2013JE004505

Gillmann, C., Chassefière, E., & Lognonné, P. (2009). A consistent picture of early hydrodynamic escape of Venus atmosphere explaining present Ne and Ar isotopic ratios and low oxygen atmospheric content. *Earth and Planetary Science Letters*, *286*(3–4), 503–513. https://doi.org/10.1016/j.epsl.2009.07.016

Gillmann, C., Golabek, G. J., & Tackley, P. J. (2016). Effect of a single large impact on the coupled atmosphere-interior evolution of Venus. *Icarus*, *268*, 295–312.

https://doi.org/10.1016/j.icarus.2015.12.024

Gubbins, D., & Davies, C. J. (2013). The stratified layer at the core–mantle boundary caused by barodiffusion of oxygen, sulphur and silicon. *Physics of the Earth and Planetary Interiors*, *215*, 21–28. https://doi.org/10.1016/j.pepi.2012.11.001

Hamano, K., Abe, Y., & Genda, H. (2013). Emergence of two types of terrestrial planet on solidification of magma ocean. *Nature*, *497*(7451), 607–10. https://doi.org/10.1038/nature12163

Helffrich, G. (2014). Outer core compositional layering and constraints on core liquid transport properties. *Earth and Planetary Science Letters*, *391*, 256–262. https://doi.org/10.1016/j.epsl.2014.01.039

Hirose, K., Labrosse, S., & Hernlund, J. (2013). Composition and State of the Core. *Annual Review of Earth and Planetary Sciences*, *41*(1), 657–691. https://doi.org/10.1146/annurev-earth-050212-124007

Holmström, E., Stixrude, L., Scipioni, R., & Foster, A. S. (2018). Electronic conductivity of solid and liquid (Mg, Fe)O computed from first principles. *Earth and Planetary Science Letters*, *490*, 11–19. https://doi.org/10.1016/j.epsl.2018.03.009

Ikoma, M., Elkins-Tanton, L., Hamano, K., & Suckale, J. (2018). Water Partitioning in Planetary Embryos and Protoplanets with Magma Oceans. *Space Science Reviews*, *214*(4), 1–28. https://doi.org/10.1007/s11214-018-0508-3

Jacobson, S. A., Rubie, D. C., Hernlund, J., Morbidelli, A., & Nakajima, M. (2017). Formation, stratification, and mixing of the cores of Earth and Venus. *Earth and Planetary Science Letters*, *474*, 375–386. https://doi.org/10.1016/j.epsl.2017.06.023

Kaula, W. (1999). Constraints on Venus Evolution from Radiogenic Argon. *Icarus*, *139*(1), 32–39. https://doi.org/10.1006/icar.1999.6082

Konôpková, Z., McWilliams, R. S., Gómez-Pérez, N., & Goncharov, A. F. (2016). Direct measurement of thermal conductivity in solid iron at planetary core conditions. *Nature*, *534*(7605), 99–101. https://doi.org/10.1038/nature18009

Konopliv, A. S., & Yoder, C. F. (1996). Venusian k2 tidal Love number from Magellan and PVO tracking data. *Geophysical Research Letters*, *23*(14), 1857–1860. https://doi.org/10.1029/96gl01589

Korenaga, J. (2008). Urey ratio and the structure and evolution of Earth's mantle. *Reviews of Geophysics*, *46*(2), RG2007. https://doi.org/10.1029/2007RG000241

Labrosse, S. (2015). Thermal evolution of the core with a high thermal conductivity. *Physics of the Earth and Planetary Interiors*, *247*, 36–55. https://doi.org/10.1016/j.pepi.2015.02.002

Labrosse, S., Hernlund, J. W., & Coltice, N. (2007). A crystallizing dense magma ocean at the

base of the Earth's mantle. *Nature*, *450*(7171), 866–9. https://doi.org/10.1038/nature06355

Landeau, M., Aubert, J., & Olson, P. (2017). The signature of inner-core nucleation on the geodynamo. *Earth and Planetary Science Letters*, *465*, 193–204. https://doi.org/10.1016/j.epsl.2017.02.004

Laneuville, M., Hernlund, J., Labrosse, S., & Guttenberg, N. (2017). Crystallization of a compositionally stratified basal magma ocean. *Physics of the Earth and Planetary Interiors*. https://doi.org/10.1016/j.pepi.2017.07.007

Lay, T., Hernlund, J., & Buffett, B. A. (2008). Core–mantle boundary heat flow. *Nature Geoscience*, *1*(1), 25–32. https://doi.org/10.1038/ngeo.2007.44

Li, M., McNamara, A. K., Garnero, E. J., & Yu, S. (2017). Compositionally-distinct ultra-low velocity zones on Earth's core-mantle boundary. *Nature Communications*, *8*(1). https://doi.org/10.1038/s41467-017-00219-x

McKinnon, W. B., Zhanle, K. J., Ivanov, B. D., & Melosh, J. H. (1997). Cratering on Venus: Models and observations. In *Venus II* (pp. 969–1014). University of Arizona Press.

Mosenfelder, J. L., Asimow, P. D., & Ahrens, T. J. (2007). Thermodynamic properties of Mg2SiO4 liquid at ultra-high pressures from shock measurements to 200 GPa on forsterite and wadsleyite. *Journal of Geophysical Research: Solid Earth*, *112*(6). https://doi.org/10.1029/2006JB004364

Nakagawa, T. (2018). On the thermo-chemical origin of the stratified region at the top of the Earth's core. *Physics of the Earth and Planetary Interiors*, *276*, 172–181. https://doi.org/10.1016/j.pepi.2017.05.011

Nakagawa, T., & Tackley, P. J. (2010). Influence of initial CMB temperature and other parameters on the thermal evolution of Earth's core resulting from thermochemical spherical mantle convection. *Geochemistry Geophysics Geosystems*, *11*(6). https://doi.org/10.1029/2010GC003031

Nakagawa, T., & Tackley, P. J. (2015). Influence of plate tectonic mode on the coupled thermochemical evolution of Earth's mantle and core. *Geochemistry Geophysics Geosystems*, *16*, 3400–3413. https://doi.org/10.1002/2015GC005996

Nakajima, M., & Stevenson, D. J. (2015). Melting and mixing states of the Earth's mantle after the Moon-forming impact. *Earth and Planetary Science Letters*, *427*, 286–295. https://doi.org/10.1016/j.epsl.2015.06.023

Namiki, N., & Solomon, S. C. (1998). Volcanic degassing of argon and helium and the history of crustal production on Venus. *Journal of Geophysical Research*, *103*(E2), 3655. https://doi.org/10.1029/97JE03032

Nimmo, F. (2015). Thermal and Compositional Evolution of the Core. In *Treatise on Geochemistry: Second Edition* (Vol. 9, pp. 217–241). Elsevier B.V.

https://doi.org/10.1016/B978-044452748-6.00147-4

O'Rourke, J. G., & Korenaga, J. (2015). Thermal evolution of Venus with argon degassing. *Icarus*, *260*, 128–140. https://doi.org/10.1016/j.icarus.2015.07.009

O'Rourke, J. G., & Shim, S. -H. (2019). Hydrogenation of the Martian Core by Hydrated Mantle Minerals With Implications for the Early Dynamo. *Journal of Geophysical Research: Planets*, 2019JE005950. https://doi.org/10.1029/2019JE005950

O'Rourke, J. G., & Stevenson, D. J. (2016). Powering Earth's dynamo with magnesium precipitation from the core. *Nature*, *529*(7586), 387–389. https://doi.org/10.1038/nature16495

O'Rourke, J. G., Korenaga, J., & Stevenson, D. J. (2017). Thermal evolution of Earth with magnesium precipitation in the core. *Earth and Planetary Science Letters*, *458*, 263–272. https://doi.org/10.1016/j.epsl.2016.10.057

O'Rourke, J. G., Gillmann, C., & Tackley, P. (2018). Prospects for an ancient dynamo and modern crustal remanent magnetism on Venus. *Earth and Planetary Science Letters*, *502*, 46–56. https://doi.org/10.1016/j.epsl.2018.08.055

O'Rourke, J. G., Buz, J., Fu, R. R., & Lillis, R. J. (2019). Detectability of Remanent Magnetism in the Crust of Venus. *Geophysical Research Letters*, *46*, 2019GL082725. https://doi.org/10.1029/2019GL082725

Ohta, K., Yagi, T., Taketoshi, N., Hirose, K., Komabayashi, T., Baba, T., et al. (2012). Lattice thermal conductivity of MgSiO3 perovskite and post-perovskite at the core-mantle boundary. *Earth and Planetary Science Letters*, *349–350*, 109–115. https://doi.org/10.1016/j.epsl.2012.06.043

Ohta, K., Kuwayama, Y., Hirose, K., Shimizu, K., & Ohishi, Y. (2016). Experimental determination of the electrical resistivity of iron at Earth's core conditions. *Nature*, *534*(7605), 95–98. https://doi.org/10.1038/nature17957

Pozzo, M., Davies, C., Gubbins, D., & Alfè, D. (2019). FeO Content of Earth's Liquid Core. *Physical Review X*, *9*(4), 041018. https://doi.org/10.1103/PhysRevX.9.041018

Rubie, D. C., Jacobson, S. A., Morbidelli, A., O'Brien, D. P., Young, E. D., de Vries, J., et al. (2015). Accretion and differentiation of the terrestrial planets with implications for the compositions of early-formed Solar System bodies and accretion of water. *Icarus*, *248*, 89–108. https://doi.org/10.1016/j.icarus.2014.10.015

Scipioni, R., Stixrude, L., & Desjarlais, M. P. (2017). Electrical conductivity of SiO2 at extreme conditions and planetary dynamos. *Proceedings of the National Academy of Sciences of the United States of America*, *114*(34), 9009–9013. https://doi.org/10.1073/pnas.1704762114

Smrekar, S. E., Davaille, A., & Sotin, C. (2018). Venus Interior Structure and Dynamics. *Space Science Reviews*, *214*(5), 88. https://doi.org/10.1007/s11214-018-0518-1

Soubiran, F., & Militzer, B. (2018). Electrical conductivity and magnetic dynamos in magma oceans of Super-Earths. *Nature Communications*, *9*(1). https://doi.org/10.1038/s41467-018-06432-6

Stevenson, D. J. (2003). Planetary magnetic fields. *Earth and Planetary Science Letters*, *208*(1–2), 1–11. https://doi.org/10.1016/S0012-821X(02)01126-3

Stixrude, L., & Karki, B. (2005). Structure and Freezing of MgSiO3 Liquid in Earth's Lower Mantle. *Science*, *310*(5746), 297–299. https://doi.org/10.1126/science.1116952

Tang, F., Taylor, R. J. M., Einsle, J. F., Borlina, C. S., Fu, R. R., Weiss, B. P., et al. (2019). Secondary magnetite in ancient zircon precludes analysis of a Hadean geodynamo. *Proceedings of the National Academy of Sciences*, *116*(2), 407–412. https://doi.org/10.1073/pnas.1811074116

Ulvrová, M., Labrosse, S., Coltice, N., Råback, P., & Tackley, P. J. (2012). Numerical modelling of convection interacting with a melting and solidification front: Application to the thermal evolution of the basal magma ocean. *Physics of the Earth and Planetary Interiors*, *206–207*, 51–66. https://doi.org/10.1016/j.pepi.2012.06.008

Way, M. J., Del Genio, A. D., Kiang, N. Y., Sohl, L. E., Grinspoon, D. H., Aleinov, I., et al. (2016). Was Venus the first habitable world of our solar system? *Geophysical Research Letters*, *43*(16), 8376–8383. https://doi.org/10.1002/2016GL069790

Weiss, B. P., Maloof, A. C., Tailby, N., Ramezani, J., Fu, R. R., Hanus, V., et al. (2015). Pervasive remagnetization of detrital zircon host rocks in the Jack Hills, Western Australia and implications for records of the early geodynamo. *Earth and Planetary Science Letters*, *430*, 115–128. https://doi.org/10.1016/j.epsl.2015.07.067

Weller, M. B., & Kiefer, W. S. (2019). The Physics of Changing Tectonic Regimes: Implications for the Temporal Evolution of Mantle Convection and the Thermal History of Venus. *Journal of Geophysical Research: Planets*, 2019JE005960. https://doi.org/10.1029/2019JE005960

Xie, S., & Tackley, P. J. (2004). Evolution of helium and argon isotopes in a convecting mantle. *Physics of the Earth and Planetary Interiors*, *146*(3–4), 417–439. https://doi.org/10.1016/j.pepi.2004.04.003

Yoder, C. F. (1995). Venus' Free Obliquity. *Icarus*, *117*(2), 250–286. https://doi.org/10.1006/icar.1995.1156

Zhang, Z., Dorfman, S. M., Labidi, J., Zhang, S., Li, M., Manga, M., et al. (2016). Primordial metallic melt in the deep mantle. *Geophysical Research Letters*, *43*(8), 3693–3699. https://doi.org/10.1002/2016GL068560

Ziegler, L. B., & Stegman, D. R. (2013). Implications of a long-lived basal magma ocean in generating Earth's ancient magnetic field. *Geochemistry, Geophysics, Geosystems*, *14*(11), 4735–4742. https://doi.org/10.1002/2013GC005001

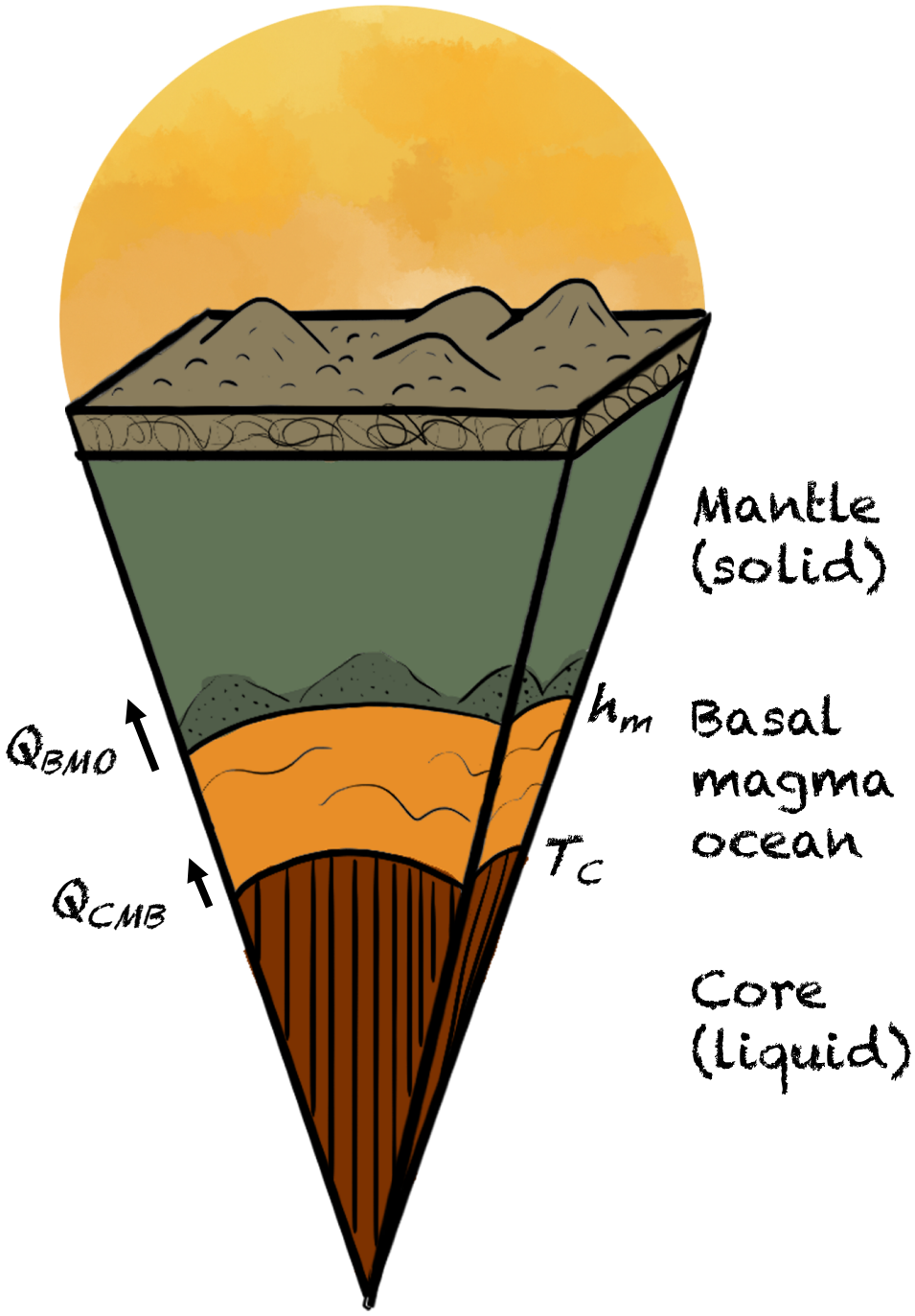

Figure 1. Cartoon of the internal structure of Venus. Four key parameters control the thermal evolution and any dynamo: the heat flow from the basal magma ocean to the solid mantle (Q_{BMO}), the heat flow across the core/mantle boundary (Q_{CMB}), the temperature at the core/mantle boundary (T_C), and the height of the basal magma ocean measured from the core/mantle boundary (h_M). Illustration by JoAnna Wendel.

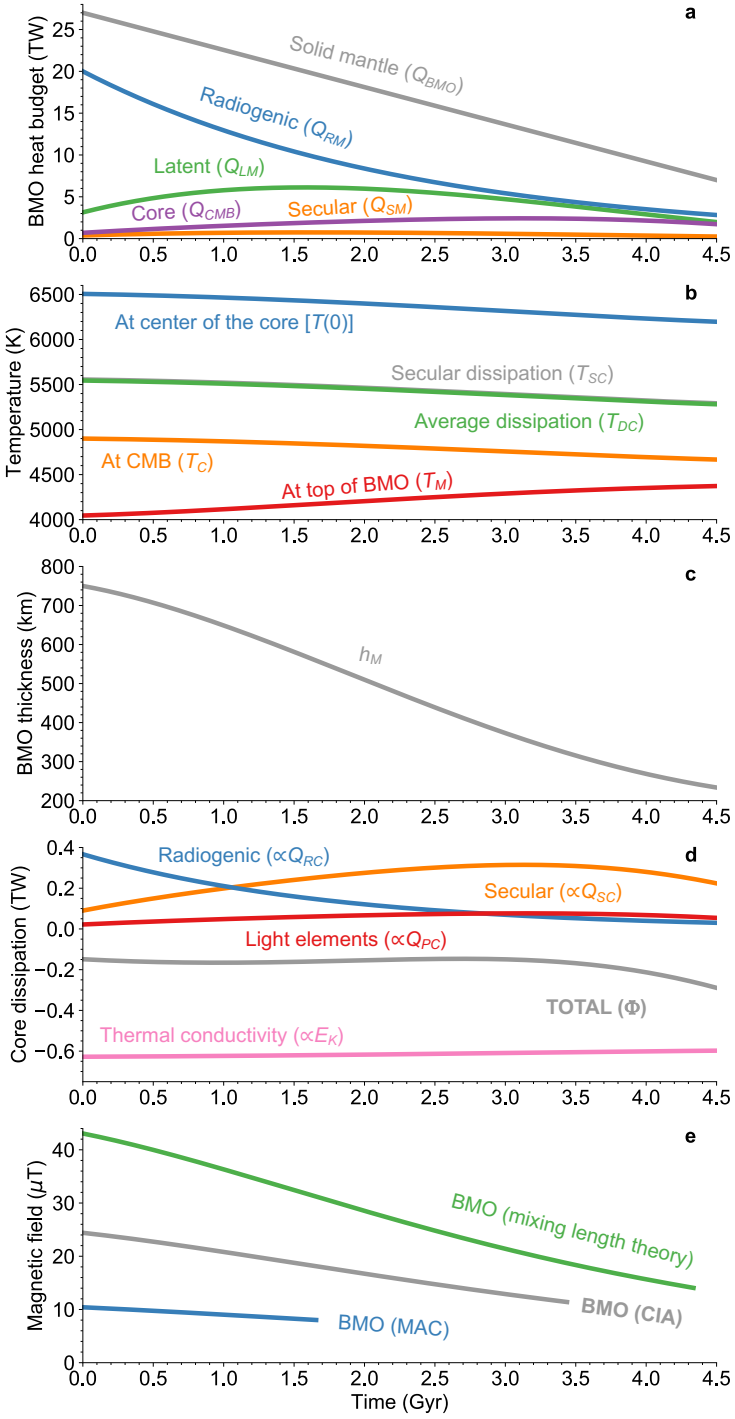

Figure 2. Nominal model for Venus. A long-lived basal magma ocean is the natural outcome of slow cooling through the solid mantle. (a) Heat budget of the basal magma ocean. (b) Temperatures at the core/mantle boundary and deeper in the core. (c) Thickness of the basal magma ocean. (d) Dissipation budget for the core including all non-zero terms. (e) Estimated strength of the surface magnetic field from three scalings.

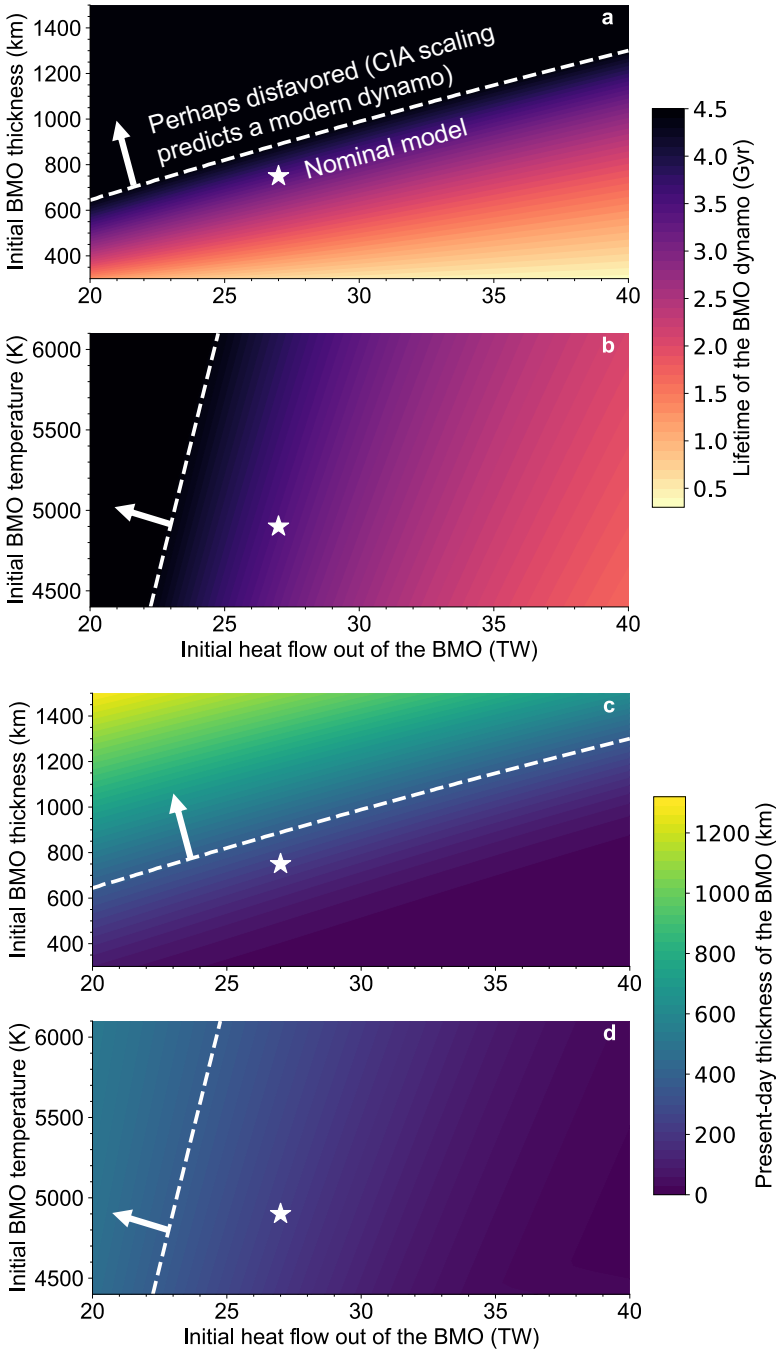

Figure 3. Sensitivity analysis for models of Venus. Lifetimes of the dynamo in the basal magma ocean are estimated with the Coriolis-Inertial-Archimedean velocity scaling using the initial heat flow to the solid mantle and the initial (a) temperature and (b) thickness of the basal magma ocean. Melt layers thicker than ~400 km are predicted to host a strong dynamo today, conflicting with observations, although the critical thickness is highly sensitive to the choice of velocity scaling. Arrows and dashed white lines indicate the potentially disfavored parameter space. Present-day thicknesses of the basal magma ocean are reported versus its initial (c) temperature and (d) thickness. White stars represent the nominal model.

Geophysical Research Letters

Supporting Information for

Venus: A Thick Basal Magma Ocean May Exist Today

J. G. O'Rourke

School of Earth and Space Exploration, Arizona State University, Tempe, AZ, USA

Contents of this file

Text S1.

This section provides the equations that govern the models for Earth and Venus. Full descriptions are available from Labrosse et al. (2017), O'Rourke et al. (2018), and cited references therein. Wherever possible, this study copies the notation of prior publications. The code used to run the models and generate related figures is publicly available as stated in the Acknowledgements.

S1.1. General methods

The global energy budget for the coupled evolution of the BMO and the core is

$$Q_{BMO} = Q_{SM} + Q_{RM} + Q_{LM} + Q_{CMB}, \quad (S1)$$

where the heat flow across the solid/liquid interface in the basal mantle (Q_{BMO}) equals the sum of the radiogenic heating in the BMO (Q_{RM}), the secular cooling of the BMO (Q_{SM}), the latent heat released by solidification of the BMO (Q_{LM}), and the heat flow across the core/mantle boundary (Q_{CMB}). Next, the energy budget of the core is expanded as

$$Q_{CMB} = Q_{SC} + Q_{RC} + Q_{PC} + Q_{GC} + Q_{LC} + Q_{IC}, \quad (S2)$$

which includes secular cooling of the outer core (Q_{SC}), radiogenic heating (Q_{RC}), precipitation of Mg-rich minerals near the CMB (Q_{PC}), and three terms associated with the growth of an inner core: gravitational energy from excluded light elements (Q_{GC}), latent heat (Q_{LC}), and conductive cooing (Q_{IC}). Combining the contributions from individual isotopes in the BMO,

$$Q_{RM} = Q_{RM}(0) \exp[-\lambda_M t], \quad (S3)$$

where $Q_{RM}(0)$ is the initial radiogenic heat production in the BMO and λ_M is an average decay constant. Crucially, we assume that heat-producing elements are incompatible in the solidifying mantle so the volumetric heating rate in the BMO increases over time. Assuming that potassium is the only source of radiogenic heat in the core,

$$Q_{RC} = M_C H_K [K]_C \exp(-\lambda_C t), \quad (S4)$$

where M_C is the mass of the core, H_K is the initial radiogenic heat production per unit mass per ppm of potassium, $[K]_C$ is the abundance of potassium in the core, and λ_M is the decay constant for potassium-40.

All other terms on the right-hand sides of Eq. 1 and 2 are proportional to the cooling rate of the core and BMO (Labrosse, 2015; O'Rourke et al., 2018). That is,

$$Q_i = \tilde{Q}_i \left(\frac{dT_C}{dt}\right). \quad (S5)$$

Combining Eq. 1, 2, and 5 yields

$$\frac{dT_C}{dt} = \frac{Q_{BMO} - Q_{RM} - Q_{RC}}{\tilde{Q}_{SM} + \tilde{Q}_{LM} + \tilde{Q}_{SC} + \tilde{Q}_{PC} + \tilde{Q}_{GC} + \tilde{Q}_{LC} + \tilde{Q}_{IC}}. \quad (S6)$$

Crucially, the numerator of the right side of this equation is easily calculated from the imposed boundary condition for the model (Q_{BMO}) and two initial conditions (Q_{RM} and Q_{RC}). The key to obtaining a thermal history is then to write the proportionalities in the denominator as functions of the thermodynamic properties of the BMO and the core (Labrosse, 2015).

S1.1.1. Evolution of the BMO

S1.1.1.1. Heat budget

The boundary condition for the model is the heat flow out of the BMO into the solid mantle (Q_{BMO}), which we impose as a linear function of time:

$$Q_{BMO}(t) = Q_{BMO}(t_p) + \Delta Q_{BMO}\left(\frac{t - t_p}{t_p}\right), \quad (S7)$$

where t_p is the time at present day. The resultant rate of secular cooling in the BMO is

$$\tilde{Q}_{SM} = -M_M C_M, \quad (S8)$$

where M_M is the mass of the basal magma ocean and C_M is its specific heat (Labrosse et al., 2007).

The solidification rate of the BMO is directly proportional to its cooling rate. We assume a linear phase diagram: $T_C = T_A - (T_A - T_B)\phi_L$, where ϕ_L is the concentration of the Fe-rich endmember (Labrosse et al., 2007). The liquidus temperature is T_A and T_B when ϕ_L equals 0 and 1, respectively. Differentiating both sides of that equation, $\mathrm{d}T_C/\mathrm{d}t = -(T_A - T_B)\mathrm{d}\phi_L/\mathrm{d}t$, which shows that fractional crystallization increases the Fe content of the BMO. Conservation of chemical species implies

$$\frac{d\phi_L}{dt} = -\frac{3r_B^2\Delta\phi}{r_B^3 - r_C^3}\left(\frac{dr_B}{dt}\right), \quad (S9)$$

where $\Delta\phi$ is the Fe-enrichment of the BMO relative to the solid mantle (Labrosse et al., 2007). As discussed in the main text, the solidification timescale for the BMO is highly sensitive to the assumed value of $\Delta\phi$, which is only a simple stand-in for a detailed phase diagram. Therefore,

$$\frac{dT_C}{dt} = \frac{3r_B^2\Delta\phi(T_A - T_B)}{r_B^3 - r_C^3}\left(\frac{dr_B}{dt}\right). \quad (S10)$$

Finally, the latent heat is proportional to ΔS_M, the specific entropy of melting for the BMO (Labrosse et al., 2007):

$$\tilde{Q}_{LM} = -4\pi r_B^2 \Delta S_M \rho_M T_C \left(\frac{r_B^3 - r_C^3}{3r_B^2\Delta\phi(T_A - T_B)}\right). \quad (S11)$$

S1.1.1.2. Dynamo criterion

Vigorous convection in the BMO may produce a dynamo. The magnetic Reynolds number is $\mathrm{Rm} = \mu_0 v_M h_M \sigma_M$, where μ_0 is the permittivity of free space, v_M is the convective velocity, and σ_M is electrical conductivity (Blanc et al., 2019; Ziegler & Stegman, 2013). A dynamo may exist if Rm > $O(10)$. Three expressions for v_M are available (Christensen, 2010):

$$v_{MLT} = \left(\frac{h_M Q_{BMO}}{\rho_M H_T}\right)^{\frac{1}{3}} \quad (S12)$$

from mixing length theory,

$$v_{CIA} = \left(\frac{Q_{BMO}}{\rho_M H_T}\right)^{\frac{2}{5}} \left(\frac{h_M}{\Omega}\right)^{\frac{1}{5}} \quad (S13)$$

from the Coriolis-Inertial-Archimedean (CIA) force balance, and

$$v_{MAC} = \left(\frac{Q_{BMO}}{\Omega \rho_M H_T}\right)^{\frac{1}{2}} \quad (S14)$$

from the Magnetic-Archimedean-Coriolis (MAC) force balance. Here Ω is the rotational rate of the planet and $H_T = C_M/(\alpha_M g)$ is the thermal scale height with α_M as the coefficient of thermal expansion and g as the gravitational acceleration in the BMO. The magnetic field strength within the BMO is approximately

$$B_M = (2\epsilon f_{ohm} \mu_0 \rho_M v_M^2)^{\frac{1}{2}}, \quad (S15)$$

where ε is a constant prefactor and f_{ohm} is the fraction of available power that is converted to ohmic dissipation as magnetic energy. Uncertainties in f_{ohm} and ε are substantial and degenerate. Finally, the magnetic field strength at the surface is

$$B_S = \frac{1}{7} B_M \left(\frac{r_B}{r_P}\right)^3. \quad (S16)$$

S1.1.2. Evolution of the core

S1.1.2.1. Structure and heat budget

Following many previous studies (e.g., Labrosse, 2015; O'Rourke et al., 2018, 2017), the density of the core is parameterized with a fourth-order polynomial:

$$\rho(r) = \rho_0 \left[1 - \left(\frac{r}{L_p}\right)^2 - A_p \left(\frac{r}{L_p}\right)^4\right], \quad (S17)$$

where ρ_0 is the central density, r is radial distance, $L_p = [3K/(2\pi G \rho_0^2)]^{1/2}$ is a characteristic length scale, and $A_p = 0.5K' - 1.3$ is constant. Here G is the gravitational constant, K is an effective

modulus, and K' is its effective derivative. The bulk composition of the core of Venus (e.g., the abundances of light elements such as oxygen and silicon) is unconstrained. Assuming Venus has an "Earth-like" core (O'Rourke et al. 2018), the constants in Eq. S17 are derived from a fit to PREM extrapolated to the CMB pressure of ~125 GPa (Labrosse 2015). Decreasing the assumed abundances of light elements would raise the central density but decrease the total size of the core to reproduce the bulk mass and density of Venus. The adiabatic temperature profile in the core is

$$T_a(r) = T_0\left[1 - \left(\frac{r}{L_p}\right)^2 - A_p\left(\frac{r}{L_p}\right)^4\right]^{\gamma}, \quad (S18)$$

where T_0 is the central temperature and γ is the Grüneisen parameter. Integrating these profiles over the core results in gnarly polynomial expressions for terms involved in the global energy balance. To simplify those expressions, four useful functions are defined:

$$f_c(x,\delta) = x^3\left[1 - \frac{3}{5}(\delta+1)x^2 - \frac{3}{14}(\delta+1)\left(2A_p - \delta\right)x^4\right], \quad (S19)$$

$$f_k(x) = 0.2x^5\left[1 + \frac{10}{7}\left(1+2A_p\right)x^2 + \frac{5}{9}\left(3+10A_p+4A_p^2\right)x^4\right], \quad (S20)$$

$$f_\chi(x) = x^3\left\{-\frac{1}{3}\left(\frac{r_I}{L_p}\right)^2 - \frac{1}{2}\left[1+\left(\frac{r_I}{L_p}\right)^2\right]x^2 - \frac{13}{70}x^4\right\}, \quad (S21)$$

and

$$f_\gamma(x) = x^3\left[-\frac{\Gamma}{3} + \left(\frac{1+\Gamma}{5}\right)x^2 + \left(\frac{A_p\Gamma - 1.3}{7}\right)x^4\right], \quad (S22)$$

where

$$\Gamma = \left(\frac{r_C}{L_p}\right)^2\left[1 - \frac{1}{3}\left(\frac{r_C}{L_p}\right)^2\right]. \quad (S23)$$

An inner core nucleates once the adiabatic temperature at the center of the core drops below the liquidus and grows over time. The liquidus temperature in the outer core increases with pressure but decreases as more light elements are added (Labrosse, 2015):

$$T_L(r) = T_L(0) - K\left(\frac{dT_L}{dP}\right)\left(\frac{r_I}{L_p}\right)^2 + \frac{c_0\left(\frac{dT_L}{dc}\right)}{f_c\left(\frac{r_C}{L_p}, 0, A_p\right)}\left(\frac{r_I}{L_p}\right)^3, \quad (S24)$$

where dT_L/dP and dT_L/dc are the changes in liquidus temperature with pressure and composition, respectively, and c_0 is the initial concentration of light elements in the core. Before the inner core grows, the secular cooling of the core is expressed as

$$\tilde{Q}_{SC} = -\frac{4}{3}\pi\rho_0 C_C L_p^3 f_c\left(\frac{r_C}{L_p}, \gamma\right)\left[1 - \left(\frac{r_C}{L_p}\right)^2 - A_p\left(\frac{r_C}{L_p}\right)^4\right]^{-\gamma}. \quad (S25)$$

After the inner core nucleates, the secular cooling term is more complicated (Labrosse, 2015):

$$\tilde{Q}_{SC} = -\frac{4}{3}\pi\rho_0 C_C L_p^3 \left[1 - \left(\frac{r_I}{L_p}\right)^2 - A_p\left(\frac{r_I}{L_p}\right)^4\right]^{-\gamma} \left[\frac{dT_L}{dr_I} + \frac{2\gamma T_L(r_I)\left(\frac{r_I}{L_p^2}\right)\left(1 + 2A_p\left(\frac{r_I}{L_p}\right)^2\right)}{1 - \left(\frac{r_I}{L_p}\right)^2 - A_p\left(\frac{r_I}{L_p}\right)^4}\right]\left[f_c\left(\frac{r_C}{L_p}, \gamma\right) - f_c\left(\frac{r_I}{L_p}, \gamma\right)\right]\left(\frac{dr_I}{dT_C}\right). \quad (S26)$$

The liquidus temperature at the inner core boundary is

$$T_L(r_I) = T_L(0) - \left[K\left(\frac{dT_L}{dP}\right)\left(\frac{r_I}{L_p}\right)^2 + \frac{c_0\left(\frac{dT_L}{dc}\right)r_I^3}{L_p^3 f_c\left(\frac{r_C}{L_p}, 0\right)}\right]. \quad (S27)$$

Again, this formulation assumes that the cores of Earth and Venus contain similar amounts of light elements, which depress the liquidus as inner core growth concentrates them in the liquid outer core. The liquidus is differentiated to obtain the slope of the liquidus at the inner core boundary:

$$\frac{dT_L}{dr_I} = -2\left[K\left(\frac{dT_L}{dP}\right)\left(\frac{r_I}{L_p^2}\right) + \frac{3c_0\left(\frac{dT_L}{dc}\right)r_I^2}{L_p^3 f_c\left(\frac{r_C}{L_p}, 0\right)}\right]. \quad (S28)$$

Likewise, the growth rate of the inner core is proportional to the cooling rate (Nimmo, 2015; O'Rourke et al., 2017, 2018):

$$\frac{dr_I}{dT_C} = -\frac{1}{\left(\frac{dT_L}{dP} - \frac{dT_a}{dP}\right)_{r_I}}\left(\frac{T_L(r_I)}{T_C \rho_I g_I}\right), \quad (S29)$$

where ρ_I and g_I are the density and gravitational acceleration at the inner core boundary, respectively. The adiabatic temperature gradient at the inner core boundary is $\mathrm{d}T_a/\mathrm{d}P = \gamma T_L(r_I)/K$. The gravitational energy associated with the exclusion of light elements from the inner core is

$$\tilde{Q}_{GC} = \frac{8\pi^2 G\rho_0 c_0 \alpha_I r_I^2 L_p^2}{f_c\left(\frac{r_C}{L_p}, 0\right)}\left[f_\chi\left(\frac{r_C}{L_p}\right) - f_\chi\left(\frac{r_I}{L_p}\right)\right]\left(\frac{dr_I}{dT_C}\right). \quad (S30)$$

Next, the latent heat of solidification released from the inner core is

$$\tilde{Q}_{LC} = 4\pi r_I^2 \rho_I T_L(r_I)\Delta S_C\left(\frac{dr_I}{dT_C}\right), \quad (S31)$$

where ΔS_C is the entropy of melting for the core. Assuming the inner core conducts heat efficiently, the conductive heat flow across the inner core boundary is

$$\tilde{Q}_{IC} = C_C M_I K \left(\frac{dT_L}{dP}\right)\left(\frac{2r_I}{L_p^2} + \frac{16r_I}{5L_p^5}\right)\left(\frac{dr_I}{dT_C}\right), \quad (S32)$$

where M_I is the mass of the inner core. In the core, the mass enclosed within a certain radius is

$$M(r) = \frac{4}{3}\pi\rho_0 L_p^3 f_c\left(\frac{r}{L_p}, 0\right). \quad (S33)$$

Finally, the gravitational energy produced by the precipitation of light elements at the CMB is

$$\tilde{Q}_{PC} = \frac{8}{3}\pi G\rho_0^2 L_p^5 \alpha_P P_C \left[f_\gamma\left(\frac{r_C}{L_p}\right) - f_\gamma\left(\frac{r_I}{L_p}\right)\right]. \quad (S34)$$

S1.1.2.1. Dynamo criterion

The strength of any core-hosted dynamo is predicted with scaling laws from previous studies based on the total energetic dissipation (O'Rourke et al., 2018). In contrast to the model for the BMO, convective velocities in the core are not explicitly computed. Instead, the total dissipation is calculated as $\Phi = \Phi_i + \Phi_o$, where Φ_i and Φ_o are contributions from the inner core boundary and the CMB, respectively. Each contribution includes the energetic terms from Eq. 2 multiplied by an efficiency factor (Aubert et al., 2009; Labrosse, 2015):

$$\Phi_i = \frac{T_{DC}[T_L(r_I) - T_C]}{T_L(r_I)T_C}(Q_{LC} + Q_{IC}) + \frac{T_{DC}}{T_C}(Q_{GC}) \quad (S35)$$

and

$$\Phi_o = \frac{T_{DC} - T_C}{T_C}(Q_{RC}) + \frac{T_{DC}(T_{SC} - T_C)}{T_{SC}T_C}(Q_{SC}) + \frac{T_{DC}}{T_C}(Q_{PC}) - T_{DC}E_K. \quad (S36)$$

The effective temperatures for uniform dissipation and secular cooling are, respectively,

$$T_{DC} = \frac{T(r_I)}{\left[1 - \left(\frac{r_I}{L_p}\right)^2 - A_p\left(\frac{r_I}{L_p}\right)^4\right]^\gamma}\left[\frac{f_c\left(\frac{r_C}{L_p}, 0\right) - f_c\left(\frac{r_I}{L_p}, 0\right)}{f_c\left(\frac{r_C}{L_p}, -\gamma\right) - f_c\left(\frac{r_I}{L_p}, -\gamma\right)}\right], \quad (S37)$$

and

$$T_{SC} = \frac{T(r_I)}{\left[1 - \left(\frac{r_I}{L_p}\right)^2 - A_p\left(\frac{r_I}{L_p}\right)^4\right]^\gamma}\left[\frac{f_c\left(\frac{r_C}{L_p}, \gamma\right) - f_c\left(\frac{r_I}{L_p}, \gamma\right)}{f_c\left(\frac{r_C}{L_p}, 0\right) - f_c\left(\frac{r_I}{L_p}, 0\right)}\right]. \quad (S38)$$

Although $T_{DC} \sim T_{SC}$ within <10 K, $T_{DC} < T_{SC}$ because the dissipation associated with secular cooling is generated near the CMB, meaning that secular cooling is a slightly more efficient power source for the dynamo than radiogenic heating. Gravitational energy terms (Q_{PC} and Q_{GC}) are even more efficient because those dissipation terms are not penalized by a "Carnot-like" efficiency. The entropy sink associated with thermal conduction in the core is

$$E_K = 16\pi\gamma^2 k_C L_p \left[f_k\left(\frac{r_C}{L_p}\right) - f_k\left(\frac{r_I}{L_p}\right)\right], \quad (S39)$$

where k_C is the thermal conductivity of the core. Then we define the convective power as $P = \Phi/[M_C\Omega^3(r_C - r_I)^2]$ (Aubert et al., 2009). The rms magnetic field in the core is $B_{rms} = 1.5\Omega(r_C - r_I)P^{0.34}(\rho\mu_0)^{1/2}$ (Aubert et al., 2009). Next, we calculate the gravitational potentials at the CMB, inner core boundary, and on average in the outer core as $\varphi_C = r_C g/2$, $\varphi_I = r_I^2 g/(2r_C)$, and $\varphi_{av} = 0.3(g/r_C)[(r_C^5 - r_I^5)/(r_C^3 - r_I^3)]$, respectively (Aubert et al., 2009). The mass fluxes attributable to dissipation at the inner core boundary and CMB are $F_I = \Phi_I/(\varphi_{av} - \varphi_I)$ and $F_O = \Phi_O/(\varphi_O - \varphi_{av})$, respectively, and then $f_I = F_I/(F_I + F_O)$ (Aubert et al., 2009). The ratio $b_{dip} = 7.3(1 - r_I/r_C)(1+f_I)$ expresses the strength of the internal field relative to the dipole field at the CMB. The true dipole moment (TDM) is calculated (Aubert et al., 2009):

$$\mathrm{TDM} = \frac{4\pi r_C^3}{\sqrt{2}\mu_0}\left(\frac{B_{rms}}{b_{dip}}\right). \quad (S40)$$

Finally, the magnetic field at the equator is $B_S = \mu_0 \mathrm{TDM}/(4\pi r_P^3)$.

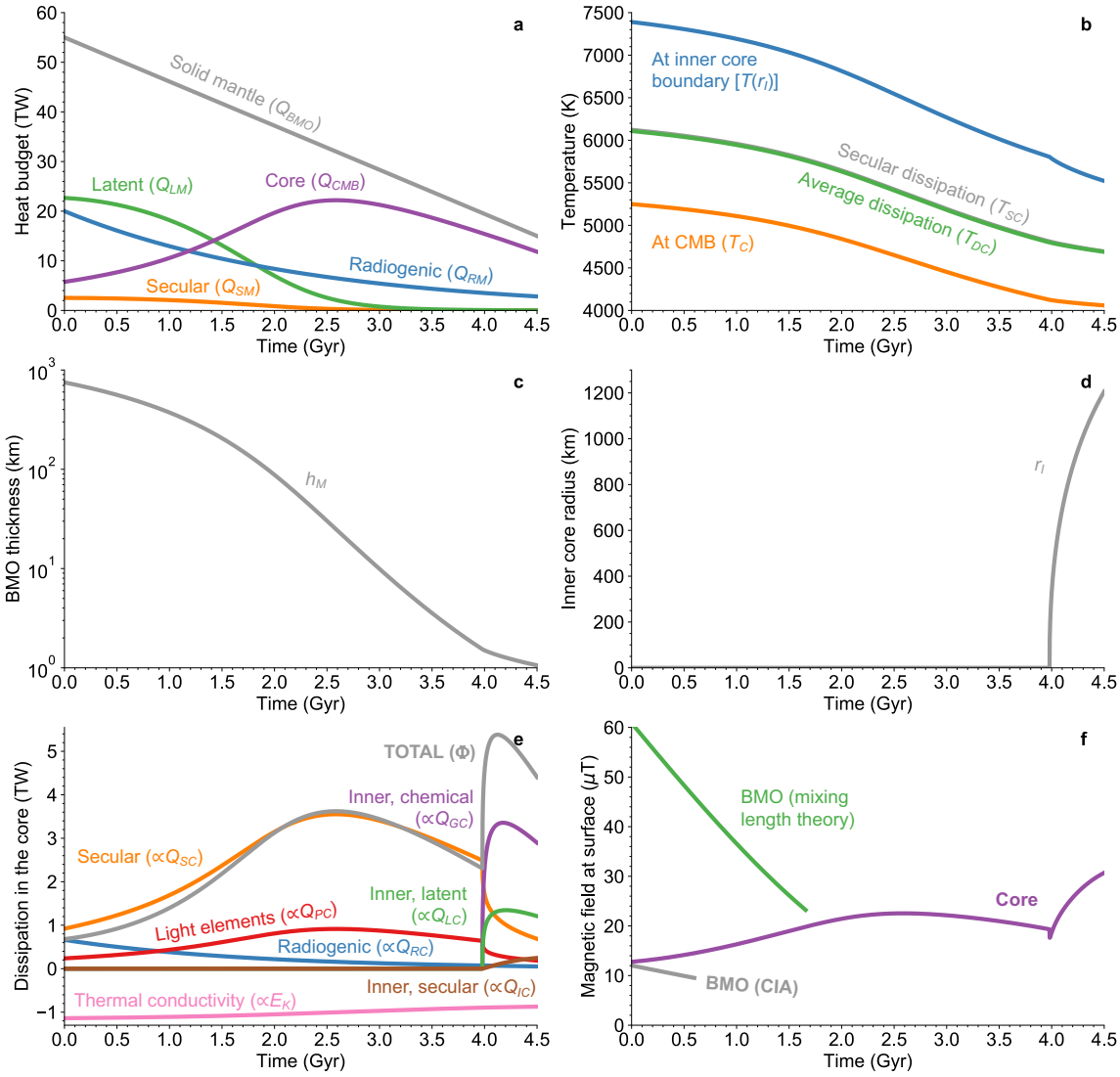

Figure S1. Nominal model for Earth discussed in Section 3.1 of the main text. A basal magma ocean survives for billions of years but is almost completely solidified at present day, which obeys seismic constraints. (a) Heat budget of the basal magma ocean. (b) Temperatures at the core/mantle boundary and deeper in the core. (c) Thickness of the basal magma ocean. (d) Radius of the inner core. (e) Dissipation budget for the core. (f) Estimated strength of the magnetic field at the surface based on the scaling law for the core and two velocity scalings for the basal magma ocean. The MAC-scaling for the basal magma ocean predicts a field strength of zero always.

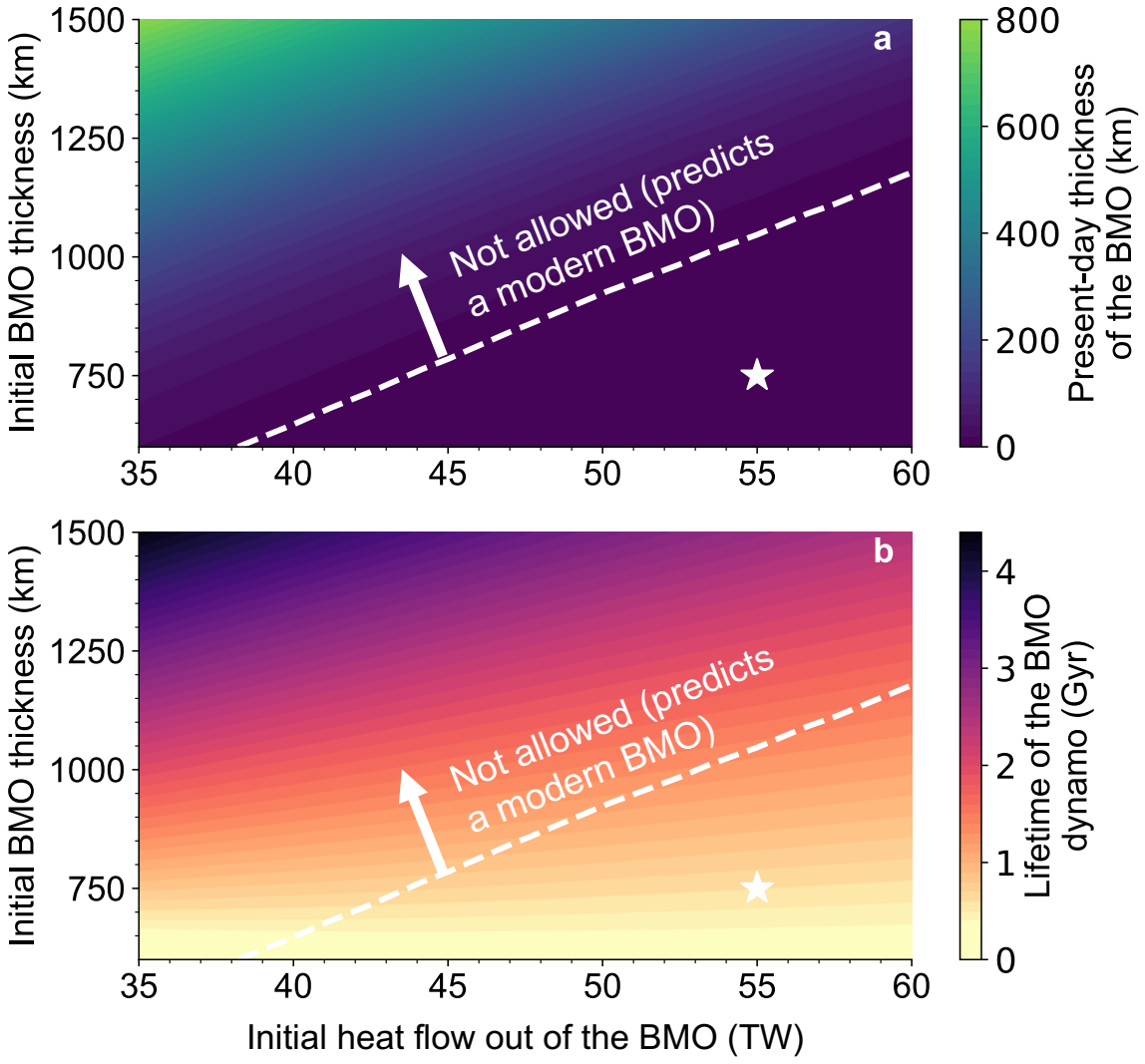

Figure S2. Sensitivity analysis for Earth discussed in Section 3.1 of the main text. The initial thickness of the basal magma ocean could have been as large as ~1000 km. Models with a thicker basal magma ocean conflict with seismic evidence against a global melt layer in the basal mantle. Arrows point towards invalid initial conditions on one side of the dashed white lines. (a) Present-day thickness of the basal magma ocean. (b) Lifetime of the dynamo in the basal magma ocean according to the Coriolis-Inertial-Archimedean scaling for flow velocity.

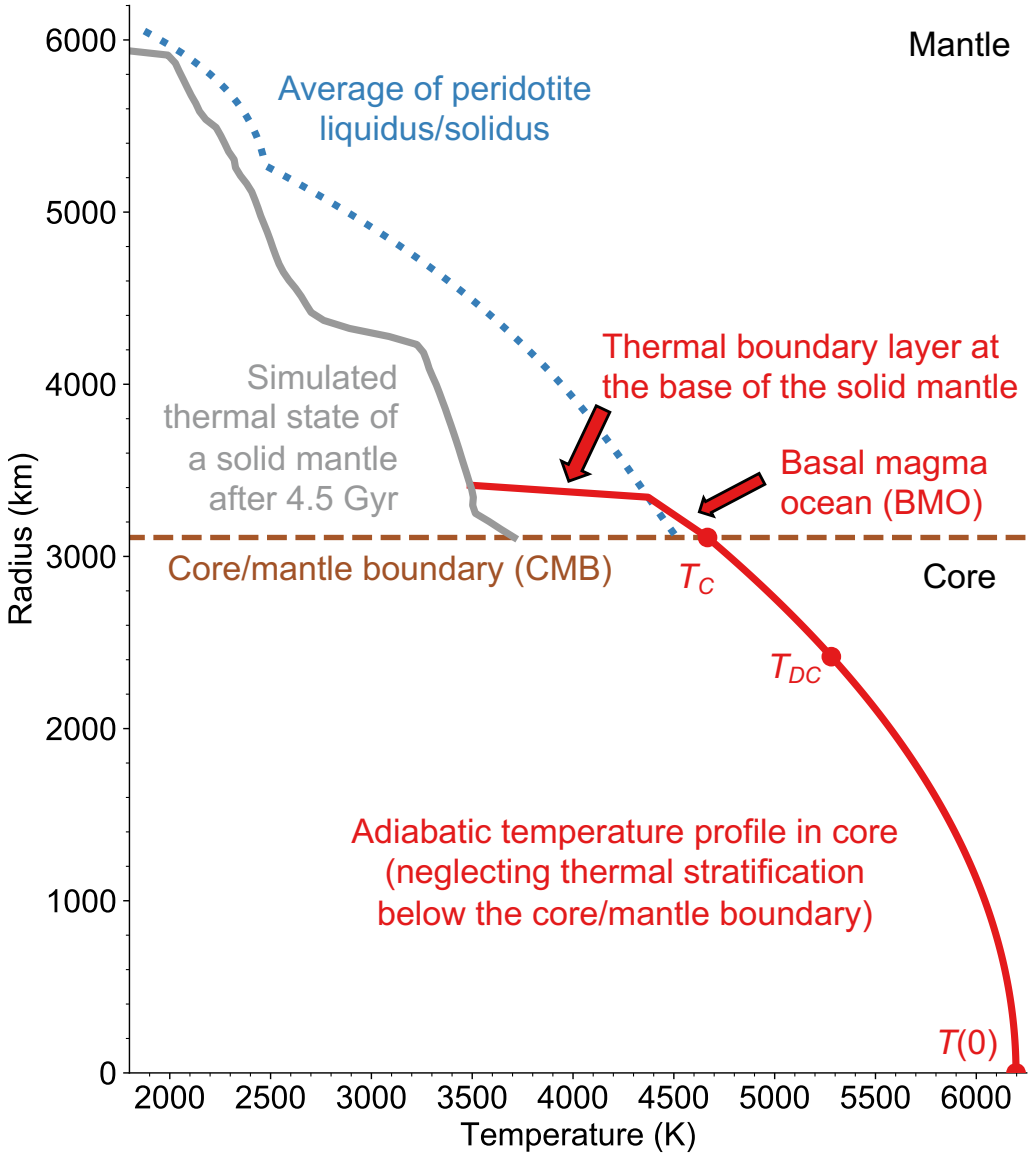

Figure S3. Sketch of the possible thermal state of the mantle at the end of the nominal model for Venus. The dotted, blue line is the average of the liquidus and solidus temperatures for peridotite (Rubie et al. 2015), which should roughly correspond to the top of any basal magma ocean. The solid, grey line is taken from the end of the preferred simulation in O'Rourke et al. (2018) in which the entire mantle is solid except perhaps for some partial melting near the base of the lithosphere. This simulation is consistent with observational constraints on crustal thickness and the history of volcanism on Venus. Red lines show how to graft our models to that thermal profile. Critically, there is always thermal boundary layer at the base of the solid mantle. An order-of-magnitude calculation suggests a thickness of ~70 km given a thermal contrast of ~300 K and a total heat flow of ~7 TW. The implied thermal gradient in the basal magma ocean is ~1.3 K/km on average, which is comparable to estimates of the adiabatic gradient. Future studies could provide self-consistent models for the thermal evolution of the entire planet.

Variable	Value	Unit	Description
Basal magma ocean			
C_M	1000	J/K/kg	Specific heat of the basal magma ocean
ΔS_M	652	J/K/kg	Entropy of melting for the basal magma ocean
$\Delta\phi$	0.088		Change in mass fraction of the Fe-rich component upon freezing
T_A	5500	K	Melting temperature of the Fe-rich component
T_B	3500	K	Melting temperature of the Mg-rich component
α_M	1.25×10^{-5}	1/K	Coefficient of thermal expansion in the basal magma ocean
σ_M	2×10^{4}	S/M	Electrical conductivity of the basal magma ocean
ε	0.63		Prefactor in the scaling law for a dynamo in the basal magma ocean
f_{ohm}	0.9		Fraction of available power that is converted into a dynamo
λ_M	1.38×10^{-17}	1/s	Average decay constant for radiogenic heating in the basal magma ocean
Core			
C_C	750	J/K/kg	Specific heat of the core
ΔS_C	127	J/K/kg	Entropy of melting for the core
γ	1.5		Grüneisen parameter
α_I	0.83		Coefficient of compositional expansion (inner core)
α_P	0.80		Coefficient of compositional expansion (light elements)
c_0	0.056		Initial mass fraction of light elements in the core
dT_L/dc	-21×10^{-3}	K	Change in liquidus temperature with composition
dT_L/dP	9×10^{-9}	K/Pa	Change in liquidus temperature with pressure
λ_C	1.76×10^{-17}	1/s	Average decay constant for radiogenic heating
H_K	4.2×10^{-14}	W/kg/ppm	Initial amount of radiogenic heating per unit mass per ppm of potassium
P_C	5×10^{-6}	1/K	Precipitation rate of light elements such as MgO and/or SiO_2 from the core

Table S1. Parameters that are held constant for both Earth and Venus. Values are taken from Labrosse et al. (2007) for the basal magma ocean and from O'Rourke et al. (2018) for the core unless otherwise noted in Text S1 or the main text.

Variable	Earth	Venus	Unit	Description
Planet				
r_P	6371	6052	km	Radius of the planet
Ω	7.27×10^{-5}	2.99×10^{-7}	1/s	Planetary rotation rate
Basal Magma Ocean				
H_T	7504	8699	km	Thermal scale height of the basal magma ocean
ρ_M	5500	5500	kg/m^3	Density of the basal magma ocean
Core				
r_C	3480	3110	km	Radius of the core
g	10.7	9.2	m/s^2	Gravitational acceleration near the core/mantle boundary
M_C	1.94×10^{24}	1.33×10^{24}	kg	Mass of the core
ρ_0	12451	11776	kg/m^3	Central density in the core
K	1403	1172	GPa	Effective modulus
K'	3.567	3.567		Derivative of the effective modulus
L_p	8049	7778	km	Length scale in the density profile
A_p	0.4835	0.4835		Constant in the density profile
P_C	125	130	GPa	Pressure at the core/mantle boundary
P_0	426	341	GPa	Effective central pressure
$T_L(0)$	5806	5124	K	Liquidus temperature at the center

Table S2. Parameters that are adjusted for application to Earth versus Venus, primarily to reflect the slight differences in internal pressures. Unless otherwise noted in Text S1 or the main text, values are taken from Labrosse et al. (2007) for Earth and O'Rourke et al. (2018) for Venus.

Variable	Units	Description
Basal Magma Ocean		
r_B	km	Radius of the upper boundary of the basal magma ocean
h_M	km	Thickness of the basal magma ocean
M_M	kg	Mass of the basal magma ocean
Q_{BMO}	TW	Heat flow out of the basal magma ocean into the solid mantle
Q_{SM}	TW	Secular cooling of the basal magma ocean
Q_{LM}	TW	Latent heat of solidification in the basal magma ocean
Q_{RM}	TW	Radiogenic heat in the basal magma ocean
T_M	K	Temperature of the top of the basal magma ocean
T_C	K	Temperature of the base of the basal magma ocean and uppermost core
v_M	m/s	Convective velocity in the basal magma ocean
Core		
r_I	km	Radius of the inner core boundary
T_{DC}	K	Average temperature in the outer core
T_{SC}	K	Effective temperature for dissipation from secular cooling
$T_L(r_I)$	K	Liquidus temperature at the inner core boundary
$[K]_C$	ppm	Abundance of potassium in the core
E_K	W/K	Entropy sink associated with thermal conduction
Q_{CMB}	TW	Total heat flow across the core/mantle boundary
Q_{SC}	TW	Secular cooling of the core
Q_{RC}	TW	Radiogenic heat in the core
Q_{PC}	TW	Gravitational energy from precipitation of light elements
Q_{GC}	TW	Gravitational energy from exclusion of light elements from the inner core
Q_{LC}	TW	Latent heat from the inner core
Q_{IC}	TW	Conductive cooling of the inner core
TDM	A m^2	True dipole moment of the core-generated magnetic field

Table S3. Key parameters that are tracked for the evolution of the basal magma ocean and core, which are defined in Text S1 and/or the main text.